DOE/ET-53088-387 IFSR #387

Effect of Shear on Toroidal Ion Temperature Gradient Mode Turbulence

B-G. Hong and *W. Horton*
Institute for Fusion Studies
The University of Texas at Austin
Austin, Texas 78712

August 1989

Effect of Shear on Toroidal Ion Temperature Gradient Mode Turbulence

B.-G. Hong and W. Horton
Institute for Fusion Studies
The University of Texas at Austin
Austin, Texas 78712

Abstract

The effect of magnetic shear on the toroidal ion temperature gradient driven drift mode is investigated through two-dimensional fluid simulations. Shear reduces the anomalous thermal transport by localizing the turbulence. Mixing length formulas for anomalous ion thermal transport are derived in various regimes with the magnetic shear.

I. Introduction

Drift wave instability driven by the ion temperature gradient has been used to explain the anomalous ion thermal conduction in tokamak experiments.[1-3] Recently, in ohmically-heated discharges in ASDEX,[1] the unsaturated linear use of the energy confinement time with density, $\tau_E \sim \bar{n}_e$ up to the density limit, was obtained. The improvement in confinement was attributed to the stabilization of η_i-mode with the peaked density profile. The peaked density profile with the pellet injection reduces η_i and results in the reduced ion thermal conduction in Alcator-C tokamak.[2] The fluctuation evidence of the existence of η_i-mode was found in TEXT experiments.[3] Density fluctuations propagating in the ion diamagnetic direction are observed through the laser scattering experiments.

The η_i-mode has been a main topic of study in recent years. The slab η_i-mode,[4-6] which is an ion acoustic wave driven by the ion temperature gradient, and the toroidal η_i-mode,[7,8] driven by the unfavorable magnetic curvature, and the ion temperature, are unstable for $\eta_i \gtrsim 1$. The correct threshold value for η_i and the growth rate requires the kinetic theory formulation which retains the full FLR effects and the resonances (ion transit and magnetic resonances) effects.[9,10] In this work, we use the improved set of fluid equations to study the effect of magnetic shear on the toroidal η_i-mode, which has been neglected in previous fluid simulations of the toroidal η_i-mode.[11,12]. For both the slab and toroidal branches, FLR-fluid equations used here give the critical (threshold) value $\eta_c \sim \frac{2}{3}$, which is a reasonable agreement with the kinetic theory calculation.[9]

In Sec. II we present the ion fluid equations with the adiabatic electron response for η_i-mode. Energy conservation relations are derived and discussed. The stability analysis is given in Sec. III. From the general dispersion relation, the analytic expressions for the growth rate, mode width, and the mixing length estimates for ion thermal conduction are

derived for both slab ($S > 2\varepsilon_n$) and toroidal ($S < 2\varepsilon_n$) η_i-mode. Results of two-dimensional fluid simulatons are presented in Sec. IV. Section V contains the summary and conclusion.

II. Model Equations

The equations describing the toroidal η_i instability used in this paper are based on the hydrodynamic ion equations assuming an adiabatic electron response. We take into account the effect of a sheared magnetic field in the region on the outside of the torus by using $\nabla_\parallel \cong i\, k_y \frac{x}{L_s}$. For the perturbed electrostatic potential ϕ, the parallel ion velocity v, and the ion pressure p, we study the following nonlinear equations;

$$(1-\nabla_\perp^2)\frac{\partial\phi}{\partial t} = -\left(1-2\varepsilon_n+\frac{1+\eta_i}{\tau}\nabla_\perp^2\right)\frac{\partial\phi}{\partial y}+2\varepsilon_n\frac{\partial p}{\partial y}$$
$$-\nabla_\parallel v+[\phi,\nabla_\perp^2\phi]-\mu_{\perp,1}\nabla_\perp^4\phi\,, \tag{1}$$

$$\frac{\partial}{\partial t}v = -\nabla_\parallel(\phi+p)-[\phi,v]+\mu_{\perp,2}\nabla_\perp^2 v\,, \tag{2}$$

$$\frac{\partial}{\partial t}p = -\frac{1+\eta_i}{\tau}\frac{\partial}{\partial y}\phi+\frac{\Gamma}{\tau}2\varepsilon_n\left(1-\frac{1}{\tau}\right)\frac{\partial\phi}{\partial y}$$
$$-\frac{\Gamma}{\tau}\frac{1+\eta_i}{\tau}\nabla_\perp^2\frac{\partial}{\partial y}\phi+\frac{2\Gamma}{\tau}2\varepsilon_n\frac{\partial}{\partial y}p-\frac{\Gamma}{\tau}\nabla_\parallel v-[\phi,p]+\kappa_\perp\nabla_\perp^2 p\,, \tag{3}$$

where $\Gamma = 5/3$ in fluid theory.

In writing Eqs. (1)–(3), we used the dimensionless variables of $(x,y)\to\rho_s(x,y)$, $z\to r_n z$ and $t\to r_n t/c_s$ with $c_s=(T_e/M_i)^{1/2}$, $\rho_s = c_s/\Omega_i$ and the scaling of the amplitude of the fields by

$$\left(\frac{e\Phi}{T_e}\,,\ \frac{v_{\parallel i}}{c_s}\,,\ \frac{\delta p_i}{p_i}\right) = \frac{\rho_s}{r_n}(\phi,v,p)\,.$$

We also include crossfield viscosities and thermal conductivity to absorb energy transformed to $|k|\to\infty$ which is outside the range of validity of the fluid equations. Values of crossfield dissipation coefficients are $\mu_{\perp,1} = 0.3\frac{T_i}{T_e}\frac{r_n}{c_s}\nu_i$, $\mu_{\perp,2} = 1.2\frac{T_i}{T_e}\frac{r_n}{c_s}\nu_i$ and $\chi_\perp = 1.33\frac{T_i}{T_e}\frac{r_n}{c_s}\nu_i$. Here ν_i is the ion-ion collision frequency.

In Eqs. (1)–(3), we assume that the dominant nonlinear terms are the $\mathbf{E}\times\mathbf{B}$ convective nonlinearities and use the Poisson bracket operator $[f,g]$ defined by $v_{\mathbf{E}}\cdot\nabla f=\hat{z}\cdot\nabla\phi\times\nabla f\equiv[\phi,f]$. Studies with nonadiabatic electron effects were made and will be reported in a later work. For the parameter used here the nonadiabatic effects are weak.

The transfer energy through Eqs. (1)–(3) is determined by the following constraints:

$$\frac{d}{dt}E_1=\frac{d}{dt}\frac{1}{2}\left\langle\phi^2+(\nabla\phi)^2\right\rangle=2\varepsilon_n\left\langle\phi\frac{\partial}{\partial y}p\right\rangle-\left\langle\phi\,\nabla_{\|}v\right\rangle-\mu_{\perp,1}\left\langle(\nabla_\perp^2\phi)^2\right\rangle \tag{4}$$

$$\frac{d}{dt}E_2=\frac{d}{dt}\frac{1}{2}\left\langle v^2\right\rangle=-\left\langle v\,\nabla_{\|}\phi\right\rangle-\left\langle v\,\nabla_{\|}p\right\rangle-\mu_{\perp,2}\left\langle(\nabla_\perp v)^2\right\rangle \tag{5}$$

$$\begin{aligned}\frac{d}{dt}E_2=\frac{d}{dt}\frac{1}{2}\left\langle p^2\right\rangle=&\left[\frac{1+\eta_i}{\tau}-\frac{\Gamma}{\tau}2\varepsilon_n\left(1-\frac{1}{\tau}\right)\right]\left\langle\phi\frac{\partial}{\partial y}p\right\rangle\\&-\frac{\Gamma}{\tau}\frac{1+\eta_i}{\tau}\left\langle p\,\nabla_\perp^2\frac{\partial}{\partial y}\phi\right\rangle-\frac{\Gamma}{\tau}\left\langle p\,\nabla_{\|}^2v\right\rangle-\kappa_\perp\left\langle(\nabla_\perp p)^2\right\rangle\ .\end{aligned} \tag{6}$$

We define the volume average by $\langle F\rangle=v^{-1}\int d^3x\,F(x,y,z,t)$. The transfer of the fluctuating energy is determined by the $\mathbf{E}\times\mathbf{B}$ flow of ion thermal heat $Q_{es}=\left\langle\phi\frac{\partial}{\partial y}p\right\rangle$, the work done by the parallel electric field on the parallel ion current, $\left\langle v\,\nabla_{\|}\phi\right\rangle$ and the work done by the flow along the ion thermal energy, $\left\langle v\,\nabla_{\|}p\right\rangle$. The total energy $E_T=E_1+E_2+\frac{\tau}{\Gamma}E_3$ satisfies

$$\begin{aligned}\frac{dE_T}{dt}=&\left(\frac{1+\eta_i}{\Gamma}+\frac{2\varepsilon_n}{\tau}\right)\left\langle\phi\frac{\partial}{\partial y}p\right\rangle-\frac{1+\eta_i}{\tau}\left\langle p\,\nabla_\perp^2\frac{\partial}{\partial y}\phi\right\rangle\\&-\mu_{\perp,1}\left\langle(\nabla_\perp^2\phi)^2\right\rangle-\mu_{\perp,2}\left\langle(\nabla_\perp v)^2\right\rangle-\kappa_\perp\left\langle(\nabla_\perp p)^2\right\rangle\ .\end{aligned} \tag{7}$$

The terms $\left\langle\phi\frac{\partial}{\partial y}p\right\rangle$ and $\left\langle p\,\nabla_\perp^2\frac{\partial}{\partial y}p\right\rangle$ correspond to the heat flux associated with $\mathbf{E}\times\mathbf{B}$ drift motion and polarization drift motion respectively. In the turbulent state the relative magnitude of these two terms are given by

$$\frac{\Gamma}{\tau}\left|\frac{\left\langle p\nabla_\perp^2\frac{\partial}{\partial y}\phi\right\rangle}{\left\langle\phi\frac{\partial}{\partial y}p\right\rangle}\right|\sim\overline{k_\perp^2}\frac{\Gamma}{\tau}\ll 1\ .$$

The other terms are from ion collision dissipation. Thus the final steady state is determined by the balance between the input from ion temperature gradient and toroidal pumping ($2\varepsilon_n Q_{es}$, and the dissipations from ion collisions.

III. Stability Analysis

The linear stability of Eqs. (1)–(3) is investigated in this section.

First, in the shearless system, the parallel ion velocity equation is decoupled from the potential and pressure equation, and the quadratic dispersion relation is

$$A\omega^2 + B\omega + C = 0 \tag{8}$$

with

$$A = (1 + k_\perp^2)$$

$$B = \left[1 - 2\varepsilon_n - \frac{1+\eta_i}{\tau}\, k_\perp^2 - \frac{4\Gamma}{\tau}\,\varepsilon_n(1+k_\perp^2)\right] k$$

$$C = \frac{2\varepsilon_n\, k^2}{\tau}\left[\eta_i + 1 - 2\Gamma + \frac{\Gamma}{\tau}\, k_\perp^2(1+\eta_i) + 2\Gamma\,\varepsilon_n\left(1+\frac{1}{\tau}\right)\right] .$$

The maximum growth rate occurs for $\frac{k_\perp^2(1+\eta_i)}{\tau} \cong 1$ and the eigenfrequency is given by

$$\omega_r + i\gamma \cong -\frac{2\Gamma}{\tau}\,\varepsilon_n k + ik\sqrt{2\varepsilon_n\,\frac{\eta_i - \eta_c}{\tau}} \tag{9}$$

with $\eta_c \sim \frac{2}{3}$. It is noted that the inclusion of the polarization (FLR) term in ion pressure equation is crucial for determining the critical ion temperature gradient, η_c, with a value comparable with the values given by kinetic theory.[9]

With the shear, we obtain the eigenmode equation from Eqs. (1)–(3),

$$\frac{d^2}{dx^2}\,\phi + Q(x)\phi = 0 \tag{10}$$

with

$$Q(x) = \frac{N}{D}\,,$$

$$N = -k_y^2 - \frac{\Omega - (1-2\varepsilon_n)}{\Omega + \frac{1+\eta_i}{\tau}} + \frac{S^2\,x^2\left[\Omega + \left(\frac{1+\eta_i}{\tau} + \frac{2\Gamma}{\tau^2}\,\varepsilon_n - \frac{\Gamma}{\tau}\,\frac{1+\eta_i}{\tau}\,k_y^2\right)\right]}{\left(\Omega + \frac{1+\eta_i}{\tau}\right)\left[\Omega\left(\Omega + \frac{4\Gamma}{\tau}\,\varepsilon_n\right) - \frac{\Gamma}{\tau}\,S^2\,x^2\right]}$$

$$-\frac{2\varepsilon_n\left[\frac{1+\eta_i}{\tau}-\frac{2\Gamma}{\tau}\varepsilon_n\left(1-\frac{1}{\tau}\right)-\frac{\Gamma}{\tau}\frac{1+\eta_i}{\tau}k_y^2\right]\Omega}{\left(\Omega+\frac{1+\eta_i}{\tau}\right)\left[\Omega\left(\Omega+\frac{4\Gamma}{\tau}\varepsilon_n\right)-\frac{\Gamma}{\tau}S^2x^2\right]},$$

$$D=1+\frac{\left(S^2x^2-2\varepsilon_n\Omega\right)\frac{\Gamma}{\tau}\frac{1+\eta_i}{\tau}}{\left(\Omega+\frac{1+\eta_i}{\tau}\right)\left[\Omega\left(\Omega+\frac{4\Gamma}{\tau}\varepsilon_n\right)-\frac{\Gamma}{\tau}S^2x^2\right]},$$

and $\Omega=\omega/\omega_{*e}=\omega/k_y$.

In Fig. 1 we compare the exponential growth rate of the time signals from the linear regime of the 2-D simulation code for Eqs. (1)–(3) with the solutions from numerical integration of the eigenmode equation (3) versus wavenumber k_y. We use the initial perturbation of the form

$$f\sim e^{-\alpha x^2}\cos(k_y\,y)$$

to determine the growth rate for typical wavenumber k_y in the initial value code. Figure 1 shows the good agreement between the two different problems so that we conclude that the 2-D simulation code with the periodic boundary condition in x,y adequately represents the effect of magnetic shear, when the box size is large compared with the eigenmode width.

The analytic expression for real frequency, growth rate and the mode width can be obtained by using the standard WKB technique. Then the eigenmode equation reduces to

$$\sigma^2\cong-\frac{S^2}{\Omega\left(\Omega+\frac{2\Gamma}{\tau}\varepsilon_n\right)}\left(1-\frac{\Gamma}{\tau}k_y^2\right)\qquad\text{for}\qquad\phi\sim e^{-\frac{1}{2}\sigma x^2}\tag{11}$$

and the dispersion relation

$$\begin{aligned}(1+k^2)\Omega^2-\left[1-2\varepsilon_n-\frac{1+\eta_i}{\tau}k^2-\frac{4\Gamma}{\tau}\varepsilon_n(1+k^2)\right]\Omega\\+\frac{2\varepsilon_n}{\tau}\left[\eta_i+1-2\Gamma+\frac{\Gamma}{\tau}k^2(1+\eta_i)+2\Gamma\,\varepsilon_n\left(1+\frac{1}{\tau}\right)\right]\\=-\sigma\left(\Omega+\frac{1+\eta_i}{\tau}\right)\left(\Omega+\frac{2\Gamma}{\tau}\varepsilon_n\right).\end{aligned}\tag{12}$$

When $S>2\varepsilon_n$, Eq. (12) reduces to the dispersion relation for shear slab, η_i-mode and

the eigenfrequency is

$$\Omega_0 = \frac{-1+i}{\sqrt{2\tau}}\, S^{1/2}(\eta_i+1)^{1/4}\left(\eta_i - \frac{2}{3}\right)^{1/4} \tag{13}$$

for $k_y^2 \cong \frac{\tau}{1+\eta_i}$ where the linear growth rate is a maximum. The effect of parallel compression, $\Gamma\nabla_{\|}\, v_{\|i}$ in the ion pressure equation is calculated using the perturbation technique, and the imaginary part of the frequency shift Ω_1 is

$$\mathrm{Im}\,\Omega_1 \cong -\frac{\Gamma}{4\tau}\, S(1+\eta_i)^{1/2}\left(\eta_i - \frac{2}{3}\right)^{-1/2} \quad \text{for} \quad k_y^2 \sim \frac{\tau}{1+\eta_i}\,. \tag{14}$$

Thus, the effect of parallel compression is stabilizing, but it is weak for the present tokamak parameters.

To estimate the level of anomalous thermal transport we use the simple mixing length formula with γ and σ evaluated at the source of the turbulence given by the fastest growing linear mode k_0. $\chi_i \sim \gamma(\Delta X)^2 \sim \frac{\gamma}{\mathrm{Re}\,\sigma}$ becomes

$$\chi_i \sim \frac{1+\eta_i}{2\tau}\, k_0 - \frac{\Gamma}{2^{5/2}\,\tau^{3/2}}\, S^{1/2}(1+\eta_i)^{5/4}\left(\eta_i - \frac{2}{3}\right)^{-3/4} k_0 \qquad \left[\frac{\rho_s}{r_n}\,\frac{cT_e}{eB}\right]\,. \tag{15}$$

The shear dependence of $\mathrm{Re}\,\sigma \sim S/|\Omega| \propto S^{1/2}$ cancels $S^{1/2}$ dependence of the growth rate γ. The validity condition for Eqs. (13)–(15) comes from the assumption $|S^2\, x^2/\Omega_0^2| < 1$ used in Eqs. (11)–(12), which is given by

$$S < \frac{\eta_i - \frac{2}{3}}{\tau}\left(\frac{\eta_i - \frac{2}{3}}{1+\eta_i}\right)^{1/2}\,. \tag{16}$$

When $2\varepsilon_n > S$, the eigenfrequency for toroidal η_i-mode is

$$\Omega = -\frac{2\Gamma}{\tau}\,\varepsilon_n + i\sqrt{2\varepsilon_n\,\frac{\eta_i - \frac{2}{3}}{\tau}} - i\,\frac{S}{2}\,\frac{\sqrt{\eta_i - \frac{2}{3}}}{\sqrt{\eta_i+1}}\,. \tag{17}$$

Effect of sheared magnetic field yields a weak stabilizing contribution to the toroidal η_i-mode.

For the mixing length formula, the anomalous transport from the toroidal η_i-mode is

$$\chi_i \sim \frac{2\varepsilon_n}{\tau S}\, k_0 \sqrt{(\eta_i+1)\left(\eta_i - \frac{2}{3}\right)} - \frac{1}{2}\, k_0 \sqrt{2\varepsilon_n\,\frac{\eta_i - \frac{2}{3}}{\tau}} \qquad \left[\frac{\rho_s}{r_n}\,\frac{cT_e}{eB}\right]\,, \tag{18}$$

The first term in Eq. (18) is the usual χ_i scaling law derived in earlier studies[7,8] and the reduction from shear effect is shown by the second term. In Eq. (18) S should be smaller than $2\varepsilon_n$ but larger than the critical shear S_*. Here we define $S_* \sim \rho_s/r_n$ such that for values of S less than S_*, Eqs. (1)–(3) are not valid and the diamagnetic frequency profile effect[13] must be taken into consideration.

When S is very small, the eigenmode equation (10) reduces to

$$\frac{d^2}{dx^2}\phi + Q(x)\phi = 0 \tag{19}$$

with

$$Q(x) = \frac{N}{D} ,$$

$$N = -k_y^2 - \frac{\Omega - (1-2\varepsilon_n)}{\Omega + \frac{1+\eta_i}{\tau}} \left(1 + \frac{x^2}{r_n^2} - \frac{\Omega \frac{x^2}{r_n^2}}{\Omega + \frac{1+\eta_i}{\tau}}\right)$$

$$- \frac{2\varepsilon_n \left[\frac{1+\eta_i}{\tau} - \frac{2\Gamma}{\tau}\varepsilon_n \left(1 - \frac{1}{\tau}\right) - \frac{\Gamma}{\tau}\frac{1+\eta_i}{\tau} k_y^2\right]}{\left(\Omega + \frac{1+\eta_i}{\tau}\right)\left(\Omega + \frac{4\Gamma}{\tau}\varepsilon_n\right)} \left(1 - \frac{\Omega \frac{x^2}{r_n^2}}{\Omega + \frac{1+\eta_i}{\tau}} - \frac{\Omega \frac{x^2}{r_n^2}}{\Omega + \frac{4\Gamma}{\tau}\varepsilon_n}\right)$$

$$D = 1 - \frac{2\varepsilon_n \frac{\Gamma}{\tau}\frac{1+\eta_i}{\tau}}{\left(\Omega + \frac{1+\eta_i}{\tau}\right)\left(\Omega + \frac{4\Gamma}{\tau}\varepsilon_n\right)} \left(1 - \frac{\Omega \frac{x^2}{r_n^2}}{\Omega + \frac{1+\eta_i}{\tau}} - \frac{\Omega \frac{x^2}{r_n^2}}{\Omega + \frac{4\Gamma}{\tau}\varepsilon_n}\right) ,$$

and $\omega_{*e} = \omega_{*e}\left(1 - \frac{\rho_s^2}{r_n^2}x^2\right)$ where $r_n = r_n(x=0)$. The lowest order eigenfrequency is given by Eq. (9) but the mode width Δx is determined by

$$(\Delta x)^2 \sim \frac{1}{\mathrm{Re}\,\sigma} \sim \tau^{5/4} \frac{\varepsilon_n^{1/4}}{(\eta_i - \eta_c)^{1/4}} \frac{r_n}{\rho_s} \quad \text{for} \quad \eta_i - \eta_c > \frac{2\Gamma^2 \varepsilon_n}{\tau} . \tag{20}$$

In the small shear limit, the mixing length estimate for the ion thermal conductivity is given by the Bohm type diffusion formula

$$\chi_i\, s \to 0 \sim \tau^{3/4} \varepsilon_n^{3/4} (\eta_i - \eta_c)^{1/4} \frac{cT_e}{eB} . \tag{21}$$

Transition formula for ion thermal conductivity is given in Hong *et al.*[9]

IV. Results of Numerical Simulations

Equations (1)–(3) are solved numerically as an initial value problem with periodic boundary conditions. In order to avoid aliasing errors, we truncate the physical domain to $(2/3)k_{\max}$.[14] The time advance scheme is the Runge-Kutta method. Typical parameters of our simulation are $\eta_i = 2, \varepsilon_n = 0.1$, $\tau = 1$, and $S = 0.0$ or 0.1 and for these parameters the maximum linear growth rate occurs at $k_x \sim 0$ and $k_y \sim 0.5$ with $\eta_c \sim \frac{2}{3}$. Simulations are performed on 64×64 grid with $L_x = L_y = 20\pi\,\rho_s$.

A. Shearless Case ($S = 0.0$)

Figure 2 shows the time evolution of the perturbed energy, E_1 and E_3 defined in Eqs. (4)–(6) for $S = 0.0$. For $S = 0.0$, ion parallel velocity equation decouples. Initially they start from Gaussian perturbation in x and y, and grow exponentially in time. After the nonlinear breaking of the exponential growth the energies grow algebraically in time. The end of linear regime and the "wave breaking" occurs at the saturation level given by the mixing length estimate which balances the mode coupling terms with the dominant linear terms driving the instability. In the quasi-steady stage, there is an energy transfer to both longer and shorter wavelengths and $E_p > E_\phi$. A slow energy transfer to short wavelengths produces a secular time growth of the fluctuation energy which is terminated by including high-k dissipation coefficients which are $\mu_\perp = 0.1$ and $\chi_\perp = 0.1$. During the linear stage, the spectrum peaks at $k_x \sim 0$ and $k_y \sim 0.5$ at which the linear growth rate has its maximum. In the final turbulent stage, however, the spectrum peaks at $k_x \sim 0.1$ $(= 2\pi\rho_s/L_x)$ and $k_y \sim 0.0$, indicating the presence of inverse cascade behavior. To obtain a true steady state the energy accumulating at $k_x = 2\pi\rho_s/L_x$ and $k_y = 0.0$ must be absorbed with a low-k dissipation mechanism.[14,15] With the inclusion of low-k dissipation models, stationary state are obtained, but the saturated rms amplitudes of fluctuating quantities and the heat flux

have a strong dependence on the low-k dissipation rates in contrast to the weak dependence on the high-k dissipations. Since the physical basis for choosing the low-k dissipation model is unclear, except for the shear model considered, we leave the low-k dissipation study of the shearless system for future studies..

In Fig. 3 the anomalous ion thermal flux q is shown against time. Numerically observed q is related to the dimensional flux Q_{es},

$$Q_{es} = \frac{\rho_s}{r_n}\frac{cT_e}{eB}\frac{p_i}{r_n}q \qquad \text{and} \qquad \chi_i = \frac{\rho_s}{r_n}\frac{cT_e}{eB}\frac{q}{1+\eta_i}\,.$$

In the turbulent state, q is of order 18 and the corresponding χ_i is of order 6.

The x-y contour plots of $\phi(\mathbf{x},t)$ and $p(\mathbf{x},t)$ in the turbulent state are shown in Fig. 4 for the reference parameters. The large scale ($\sim 20\,\rho_s$) and coherent structure between potential and pressure fluctuation are apparent. It was noted by Ottaviani *et al.*[12] that due to the coherence in the large scale structures $[\phi,p] \sim 0$, which results in an inhibition of the transport across the coherent structures. In the presence of the coherent structures the transport occurs principally along the separatrix where $\varphi \simeq 0$ as shown by Horton[16] for test particle transport in toroidal $l\eta_i$-modes.

B. With Shear

Time evolutions of the perturbed energies E_1, E_2 and E_3 of Eqs. (4)–(6) are shown in Fig. 5 with the same parameters as Fig. 2 except $S = 0.1$. "Wave breaking" occurs at lower amplitudes and in the turbulent state (quasi-steady state), rms amplitude of the fluctuations are almost 10 times smaller than $S = 0.0$ case due to the spatial localization of turbulence by magnetc shear. In the turbulent state, the potential and pressure spectrums peak at $k_x\rho_s \sim 0.2$ and $k_y\rho_s \sim 0.0$ and the velocity spectrum peaks at $k_x\rho_s \sim 0.0$ and $k_y\rho_s \sim 0.1$. With shear $S \neq 0.0$, the k_x peak of the spectrum is determined by the shear and not the box size as in the shearless case.

In Fig. 6 the anomalous thermal flux q is of order 1.5 and the resulting $\chi_i = 0.5$ which is also 10 times smaller than $S = 0.0$ case. To separate the effect of shear and toroidicity on the η_i-mode turbulence we show the effect of turning off the toroidicity parameter ε_n after $t = 170$. The effect of shear changes its role from stabilizing to destabilizing when $S > 2\varepsilon_n$ and the shear induced growth rate is given by Eqs. (13)–(14). Turning off the toroidicity strongly reduces q as we expected since the toroidal η_i-mode is dominant for $S < 2\varepsilon_n$. The potential and pressure spectrums peak at $k_x \sim 0.2$ and $k_y \sim 0.0$, but in this case ($\varepsilon_n = 0.0$) $\langle k_x^2 \rangle$ which is averaged over spectrum is bigger than in the $\varepsilon_n = 0.1$ case. The larger value of $\langle k_x^2 \rangle$ at $\varepsilon_n = 0$ results in reduced anomalous thermal flux q.

Figure 7 shows x-y contour plots of $\phi(\mathbf{x}, t)$, $v(\mathbf{x}, t)$ and $p(\mathbf{x}, t)$ in the turbulent state at time $t = 270$. The coherence between the potential and pressure fluctuations is weak compared with the $S = 0.0$ case (Fig. 4). With shear there is not the large transient overshoot of the heat flux as in Fig. 3.

V. Conclusion

Two-dimensional fluid simulations of the toroidal η_i-mode are presented with and without the magnetic shear effect. Linearly, shear provides a weak stabilizing effect on the toroidal η_i-mode. But due to the shear localization of turbulence, the saturated rms amplitudes of fluctuating quantities and the anomalous thermal flux is strongly reduced with increasing shear.

Analytic expressions for growth rate, radial mode width, and the mixing length estimate for the anomalous ion thermal flux are derived. Depending on the shear value compared with the toroidicity parameter ε_n, the final turbulent state is characterized by toroidal or sheared slab η_i-mode. When $2\varepsilon_n > S$ toroidal η_i-mode is dominant, instability and the wavenumber spectrum has a smaller $\langle k_x^2 \rangle$. When shear is very small $S < S_*$), the density and temperature profile giving the profile effect in diamagnetic drift frequency determines the radial mode

width, and resulting transport is of the Bohm-type diffusion formula (cT_e/eB) reduced by powers of ε_n and S. For the profile effect, the box size L_x can be given the physical meaning of the size of the system over which diamagnetic frequency ω_* is constant..

In the linear stage, the spectrums of fluctuating energies peak at $k_x \sim 0$ and $k_y \sim 0.5$, but the peak of the spectrum moves to longer wavelengths in the turbulent state indicating the inverse cascading behavior. For a turbulent stationary state, a low-k dissipation is necessary to advect out the energy transferred to the long wavelengths. More complicated fluid model equations which take into account the low-k dissipation have been introduced by Horton[14] and Waltz[15] but are not used here.

The x-y contour plots show the formation of large scale ($\sim 20\,\rho_s$) coherent structures with good coherence between the potential and pressure fluctuations. Across the coherent structures the transport is inhibited except by the transport along the separatrix.[16] The transport associated with the coherent structure deserves future study. Exact nonlinear dipole vortex solution for a closely related shearless system in which the $g\,\frac{n'}{n}$-driven FLR-fluid modes are linearly unstable are known.[17]

References

1. F.X. Söldner, E.R. Müller, F. Wagner, H.S. Bosch, A. Eberhagen, H.U. Fahrbach, G. Fussmann, O. Gehre, K. Gentle, J. Gernhardt, O. Gruber, W. Herrmann, G. Janeschitz, M. Kornherr, K. Krieger, H.M. Mayer, K. McCormick, H.D. Murmann, J. Neuhauser, R. Nolte, W. Poschenrieder, H. Röhr, K.-H. Steuer, U. Stroth, N. Tsois, and H. Verbeek, Phys. Rev. Lett. **61**, 1105 (1988).

2. S.M. Wolfe and M. Greenwald, Nucl. Fusion **26**, 329 (1986).

3. D.L. Brower, W.A. Peebles, S.K. Kim, N.C. Luhmann, Jr., W.M. Tang, and P.E. Phillips, Phys. Rev. Lett. **59**, 49 91987).

4. B. Coppi, M.N. Rosenbluth, and R.Z. Sagdeev, Phys. Fluids **10**, 582 (1967).

5. W. Horton, R.D. Estes, and D. Biskamp, Plasma Phys. **22**, 663 (1980).

6. G.S. Lee and P.H. Diamond, Phys. Fluids **29**, 3291 (1986).

7. W. Horton, D.-I. Choi, and W.M. Tang, Phys. Fluids **24**, 1077 (1981).

8. B.G. Hong, D.-I. Choi, and W. Horton, Phys. Fluids **29**, 1872 (1986).

9. B.G. Hong, W. Horton, and D.-I. Choi, to be published in Plasma Physics and Controlled Fusion, 1989.

10. F. Romanelli, Phys. Fluids **B1**, 1018 (1989).

11. D. Brock and W. Horton, Plasma Phys. **24**, 271 (1982).

12. M. Ottavani, F. Romanelli, R. Benzi, M. Briscolini, P. Santagelo, and S. Succi, submitted to Phys. Fluids, 1989.

13. W. Horton, D.-I. Choi, and R.D. Estes, Phys. Fluids **22**, 519 (1979).

14. W. Horton, Phys. Fluids **29**, 1491 (1986).

15. R.E. Waltz, Phys. Fluids **29**, 3684 (1986).

16. W. Horton, Phys. Fluids **23**, 1107 (1981).

17. W. Horton, J. Liu, J.D. Meiss, and J.E. Sedlak, Phys. Fluids **29**, 1004 (1986).

Figure Captions

1. Growth rate $\gamma\, c_s/r_n$ versus wavenumber $k_y\, \rho_s$ for the toroidal η_i-mode obtained from the shooting code with $\phi_{k_y}(x^2 \to \infty) \to 0$ (solid line) compared with the growth rates from the 2D simulation code (x-points). For mode width Δx_k small compared withthe box size, the agreement is good.

2. Evolution of the energies E_p and E_ϕ for the shearless system with $\eta_i = 2$, $\varepsilon_n = 0.1$, and $\tau = 1$.

3. The heat flux q for the shearless system showing the large transient peak and the chaotic dependence of $q(t)$ in the turbulent state.

4. Contours of constant levels of (a) potential ϕ and (b) pressure fluctuation δp at typical time in the turbulent state ($t = 260$) for the simulation experiment in Figs. 2 and 3.

5. Evolution of the energies E_p, E_v and E_ϕ for the same parameters in Figs. 2–4 except with shear $S = 0.1$.

6. The heat flux q for the toroidal η_i-mode with shear $S = 0.1$. The order of magnitude reduction of q from the shearless case in Fig. 3 arises from the small radial correlation length $\ell_c < 1/S$ in the sheared system. After $t = 170$, the upper curve keeps $\varepsilon_n = 0.1$ and the lower curve has $\varepsilon_n = 0.0$.

7. Contours of constant levels of (a) potential ϕ, (b) parallel ion velocity $v_{||}$ and (c) pressure fluctuation δp for a typical time ($t = 270$) in the turbulent state in Fig. 5.

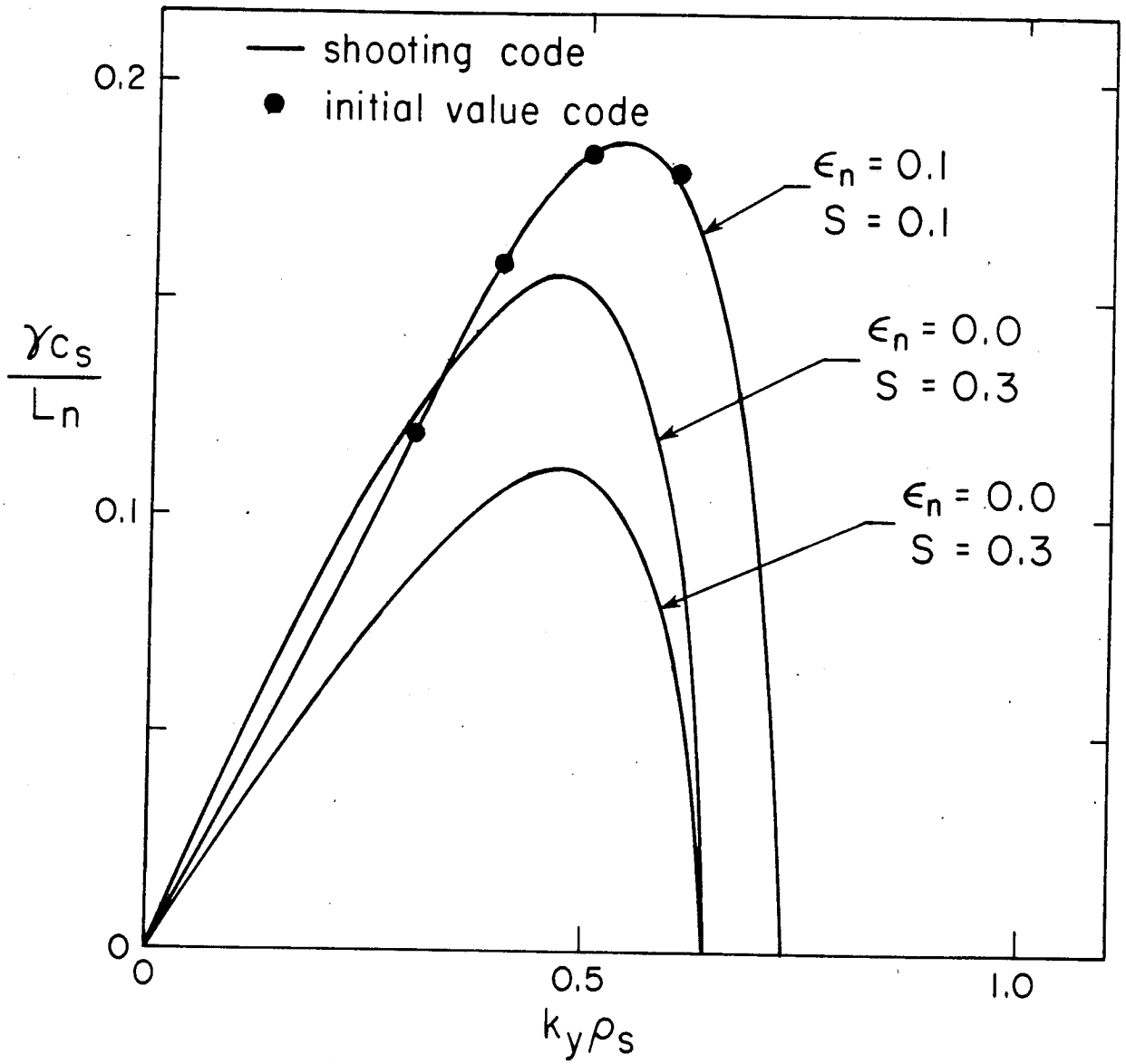
shooting code
initial value code
$\epsilon_n = 0.1$
$S = 0.1$
$\epsilon_n = 0.0$
$S = 0.3$
$\epsilon_n = 0.0$
$S = 0.3$
$\frac{\gamma c_s}{L_n}$
0.2
0.1
0
0
0.5
1.0
$k_y \rho_s$

Fig. 1

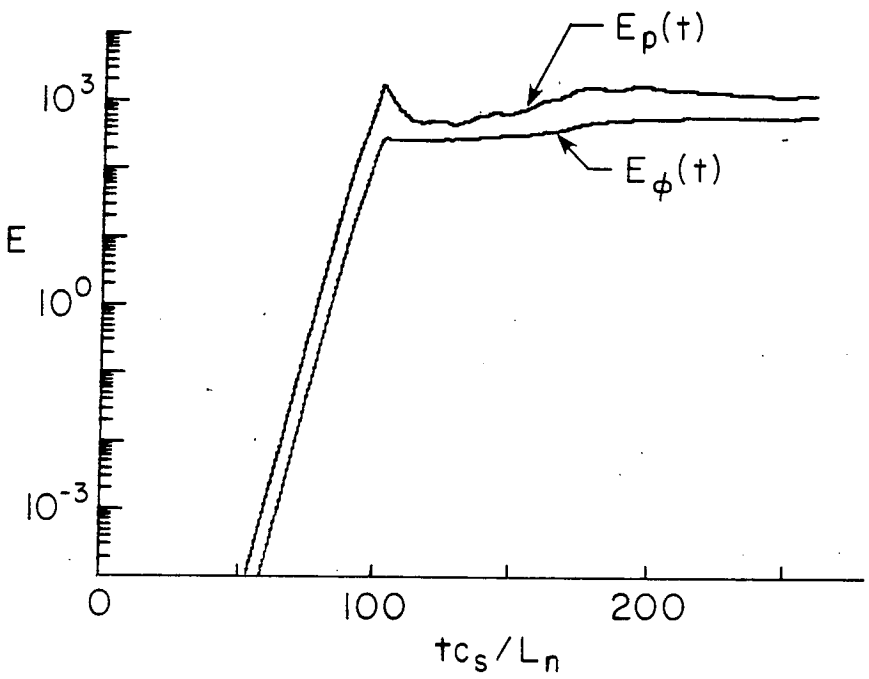

Fig. 2

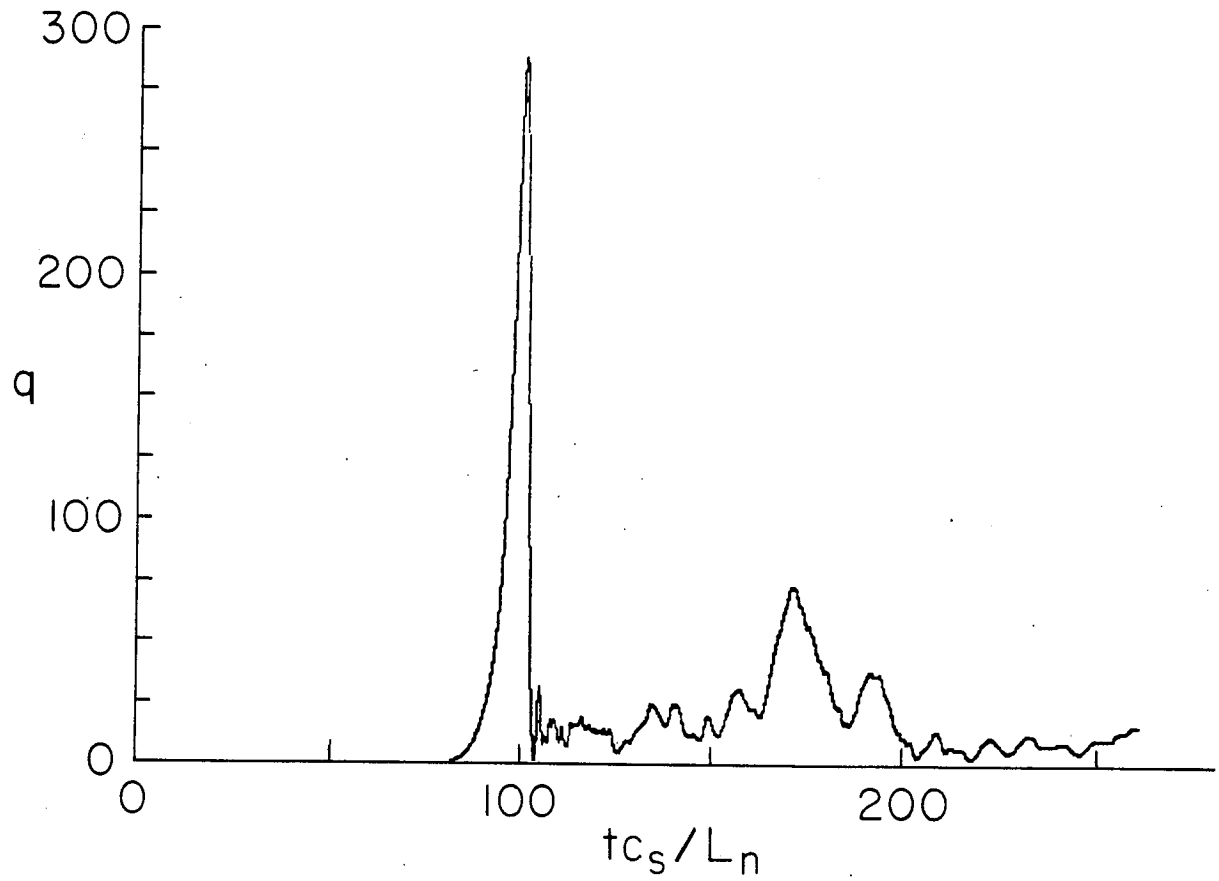

Fig. 3

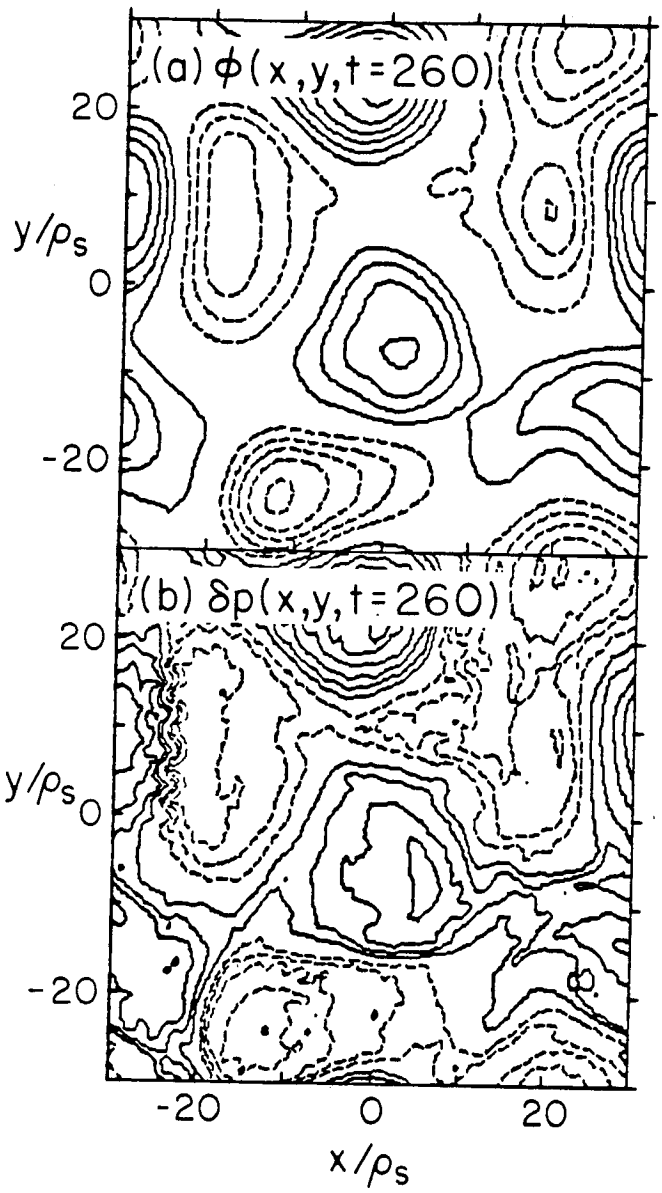

Fig. 4

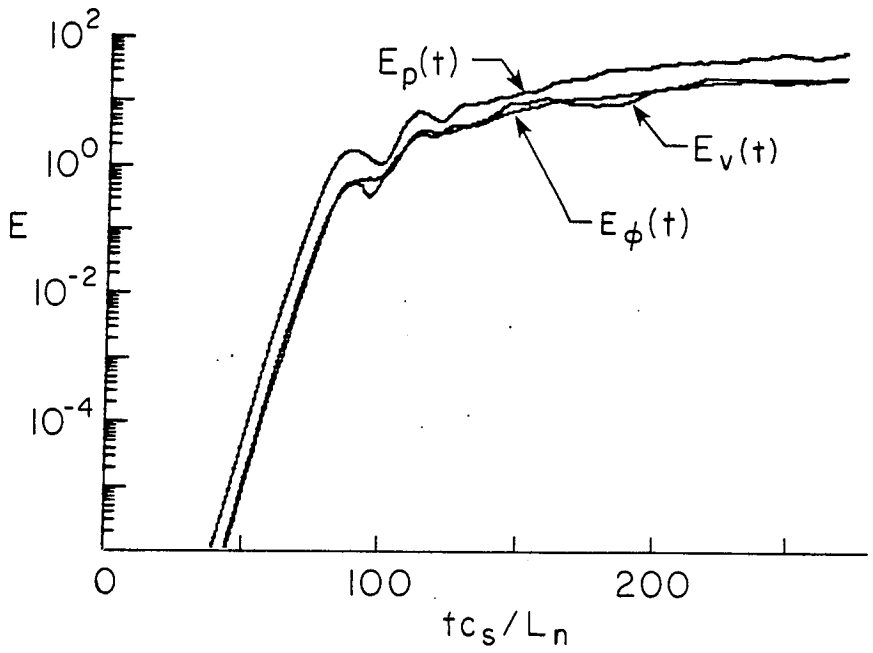

Fig. 5

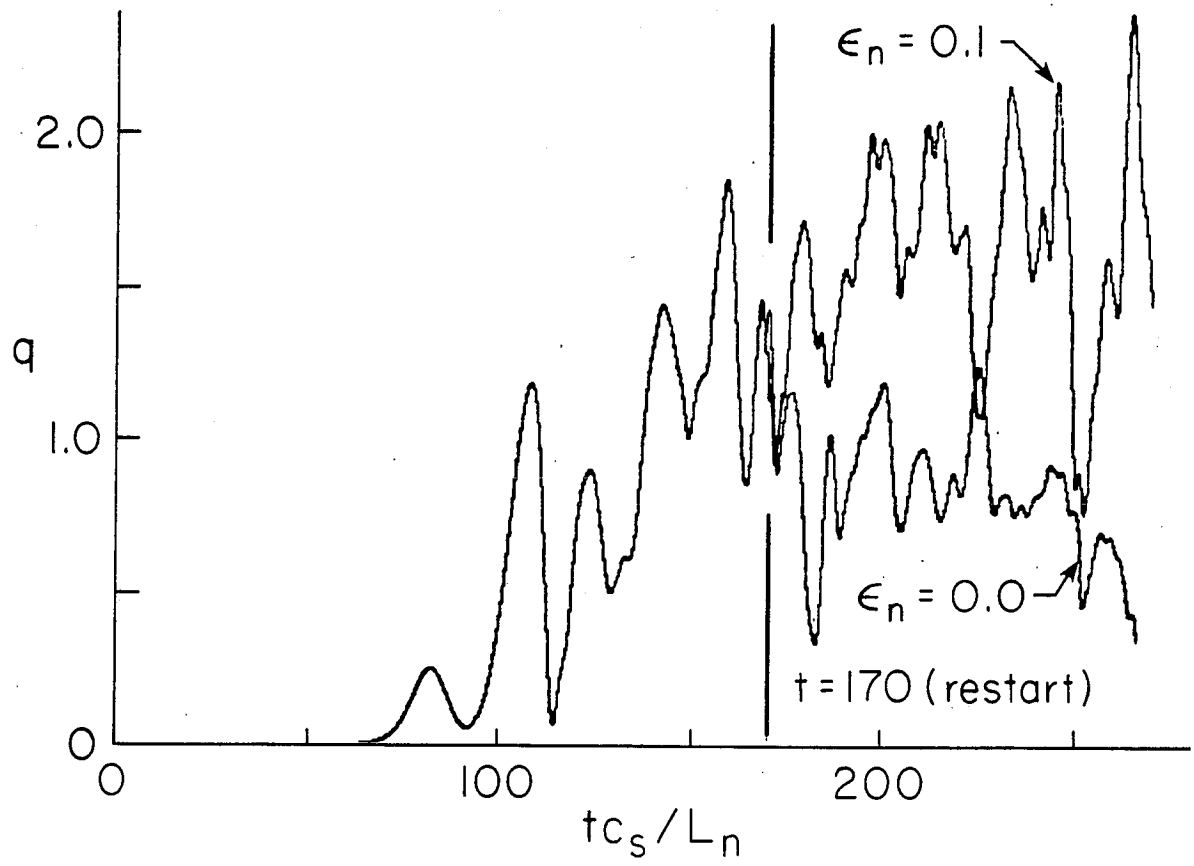

Fig. 6

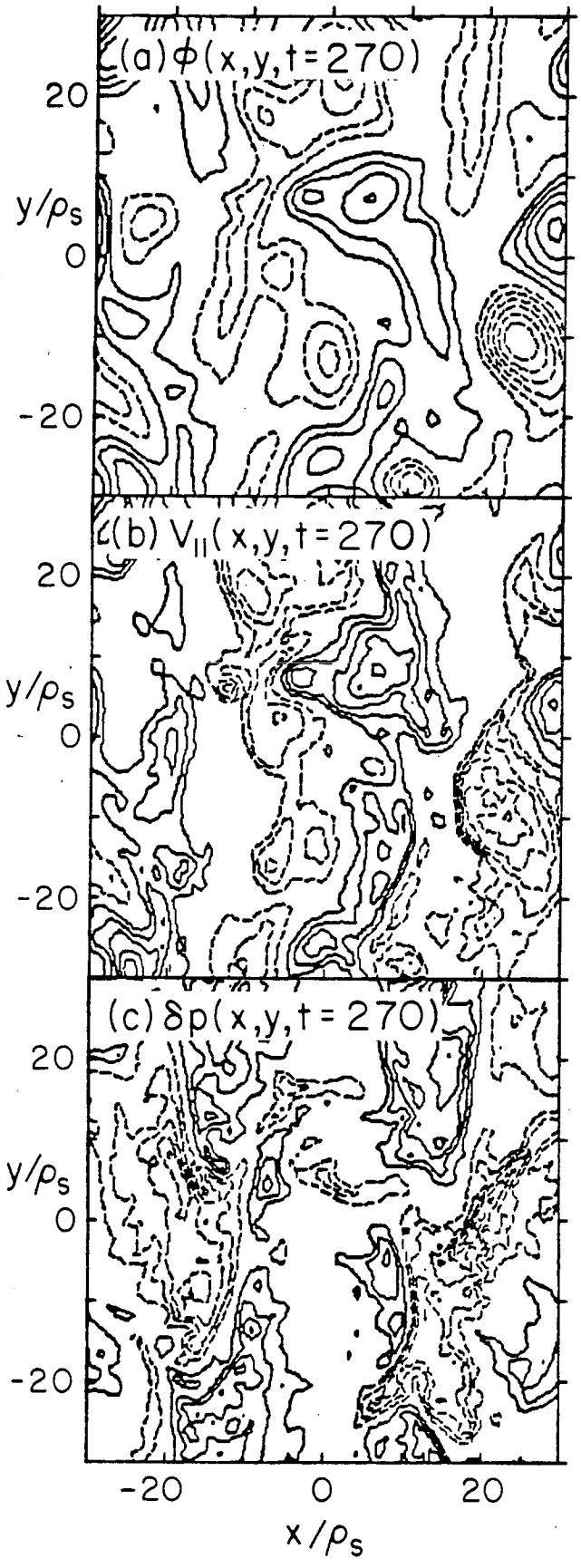

Fig. 7